

Cite this: *J. Mater. Chem. A*, 2019, 7, 25650

Hole dynamic acceleration over CdSO nanoparticles for high-efficiency solar hydrogen production with urea photolysis†

Fengting Luo,^{ab} Wen Qiao,^a Huichao He,^{id c} Xiaoyong Xu,^{id *ab} Jingguo Hu,^{*b} Yong Zhou^{id *d} and Dunhui Wang^{*ad}

Solar water splitting to hydrogen (H₂) fuel is considered a sustainable approach to meet green energy demands in the future, but is mainly limited owing to the sluggish hole dynamics involved in the water oxidation reaction and bulk charge separation. Herein, we implemented hole dynamics engineering over cadmium sulfide (CdS) nanoparticles (NPs) *via* the oxidation reaction substitution with a facile urea oxidation reaction (UOR) and surface conjugation with sulfurous groups (–S/SO_x^{2–}) as hole-extraction chains, which thermodynamically reduced the reaction barrier and kinetically accelerated the charge separation concomitantly. We then demonstrated a highly efficient photocatalytic H₂ evolution reaction (HER) from a urea solution with valuable urea degradation. An impressive and stable H₂ generation rate of 1.49 mmol h^{–1} g^{–1} was achieved under 1 sun irradiation with an apparent quantum yield (AQY) of up to 2.4% at 420 nm. In this study, we designed CdS_xO NP photocatalysts to enable hole thermodynamic and kinetic acceleration, which promise a cost-effective and course-smooth solar H₂ production along with urea-rich wastewater purification.

Received 1st August 2019
Accepted 18th October 2019

DOI: 10.1039/c9ta08357j

rsc.li/materials-a

Introduction

With increasing energy demands and climate concerns, intense efforts in developing clean and renewable energy technologies have been made to reduce fossil fuel utilization.^{1–5} Photocatalytic water splitting over semiconductors to produce green hydrogen (H₂) using renewable solar input has been considered a promising approach for future energy needs.^{6–8} Unfortunately, despite huge efforts for more than 40 years in the past, the direct photocatalysis for the overall water splitting process is still facing the dilemma of a much lower conversion efficiency. The challenge lies mainly in the four-electron water oxidation reaction (WOR) with sluggish kinetics,^{9–11} in which overcoming the thermodynamic uphill demands a large overpotential for the whole redox course. Therefore, most semiconductors appear incapable in hole dynamics toward WOR under strong competition with spontaneous charge recombination.¹²

An efficient strategy of replacing the formidable WOR with thermodynamically more favorable reactions has been reported to give rise to energy-saving H₂ production in electrochemical (EC)^{13–15} and photo-electrochemical (PEC) devices.¹⁶ Several molecules, such as oxysulfide,¹⁶ urea,¹⁷ methanol¹⁸ and hydrazine,¹⁹ have been observed to enable increased energy conversion due to their facile oxidation thermodynamics. However, the oxidation substitution has been underexplored in photocatalytic H₂ evolution decoupled from water splitting so far. Notably, the urea emitted from modern agriculture and chemical industries is one of the most common water pollutants.²⁰ Direct urea fuel cells offer great promise for energy-sustainable developments and concurrently remedying urea-rich wastewater.²¹ Urea oxidative hydrolysis requires a thermodynamic potential as low as 0.37 V,²² which is much milder than WOR. Thus, it is attractive to replace WOR with the urea oxidation reaction (UOR) for enhanced photocatalytic H₂ production and simultaneous urea-rich wastewater purification. Moreover, the six-hole UOR (*i.e.* CO(NH₂)₂ + 6OH[–] + 6h⁺ → N₂ + CO₂ + 5H₂O) can furnish abundant electrons for the H₂ evolution reaction (HER) and avoids the explosive H₂/O₂ gas mixing without low-value O₂ generation, but makes a special demand on catalysts in steering hole transfer.

Cadmium sulfide (CdS) has been considered one of the most promising photocatalysts for solar H₂ generation because of its desirable band alignment for substantial sunlight absorption and suitable redox potentials for water splitting.^{23–26} However, CdS still shows the low activity and poor stability for

^aCollege of Electronics and Information, Hangzhou Dianzi University, Hangzhou 310018, China. E-mail: xxy@yzu.edu.cn; wangdh@nju.edu.cn

^bCollege of Physics Science and Technology, Yangzhou University, Yangzhou 225002, China. E-mail: jghu@yzu.edu.cn

^cState Key Laboratory of Environmental Friendly Energy Materials, Southwest University of Science and Technology, Mianyang 621010, China. E-mail: hehuichao@swust.edu.cn

^dSchool of Physics, Nanjing University, Nanjing 210093, China. E-mail: zhouyong1999@nju.edu.cn

† Electronic supplementary information (ESI) available. See DOI: 10.1039/c9ta08357j

photocatalytic H₂ evolution due to its sluggish hole dynamics against charge recombination and anodic corrosion. Herein, we report a strategy of modulating hole dynamics over CdS nanoparticles (NPs) through conjugation with sulfurous groups (–S/SO_x^{2–}) and integration with accessible UOR, enabling an impressive solar H₂ generation with simultaneous urea degradation. The conjugated sulfurous groups serve as hole extraction channels toward UOR, evidenced by various kinetics analyses on charge separation, significantly facilitating HER with a record apparent quantum yield (AQY) of 2.4% at 420 nm for solar-to-H₂ conversion without an additional sacrificial agent.

Results and discussion

Preparation and characterization

A facile co-solvent method with a tunable ratio of Cd and S sources was used to regulate the CdS growth, followed by extraction washing and air drying, resulting in the formation of sulfurous group-conjugated CdS (CdS_xO) NPs (see Method for synthesis details, Fig. 1a). The transmission electron microscopy (TEM) image in Fig. 1b shows that the CdS_xO product appears as a flocculent colloid containing plenty of NPs with wide sizes of less than 10 nm. According to the X-ray diffraction (XRD) pattern (Fig. S1, ESI[†]) and the high-resolution TEM (HR-TEM, Fig. 1c), these NPs were identified as cubic-phase CdS crystals with resolved (111) lattice planes.²⁷ The selected area electron diffraction (SAED) and the fast Fourier transform (FFT) patterns (Fig. S2, ESI[†]) further confirm the well-defined cubic CdS crystallinity. Interestingly, the energy-dispersive X-ray

(EDX) spectrum (Fig. S3, ESI[†]) and corresponding elemental mappings (Fig. 1d) illustrate the presence of the Cd, S, and O elements in a homogeneous distribution for the CdS_xO sample. The Fourier transform infrared (FT-IR) spectra confirm that the CdS_xO NPs are conjugated with abundant sulfurous groups on the surface, as shown in Fig. 1e, where the observed absorption peaks at around 1007, 1107 and 1633 cm^{–1} can be ascribed to the –SO₃^{2–}, –SO₄^{2–} and –S groups, respectively, while absent in the commercial pure CdS crystals. The FT-IR peak identification is consistent with the previous studies,^{28,29} and moreover is further verified by controlled experiments herein (Fig. S4, ESI[†]). The Raman spectra (Fig. S5, ESI[†]) show two typical peaks at 299 and 600 cm^{–1} of cubic-phase CdS,³⁰ but the peak intensities of the CdS_xO sample are much lower than that of the pure CdS sample probably due to the shielding effect of the massive surface groups.

To further confirm the surface bonding of the sulfurous groups on the CdS_xO NPs, we set the atomic ratios of the Cd to S sources at 1 : 910 and 1 : 1 in the reaction mixture to obtain different samples (labeled as CdS_xO-1 and CdS_xO-2, respectively), and probed their surface components before and after the annealing treatment. In the absence of a sulfur-rich environment, the resulting CdS_xO-2 sample displays an obvious decline in the surface sulfurous groups compared with the CdS_xO-1 sample, as evidenced by their FT-IR spectra (Fig. S6, ESI[†]), in which the annealed CdS sample almost loses all FT-IR signals of the surface groups due to the removal of the sulfurous groups by annealing above 500 °C. In addition, their EDX elemental proportions were analyzed and are shown in Fig. S7 (ESI[†]), in which the maximum ones of the S and O elements and the minimum one of the Cd element appear in the CdS_xO-1 sample. The X-ray photoelectron spectra (XPS, Fig. S8, ESI[†]) exhibit the characteristic peaks of S 2p and Cd 3d in the Cd–S coordination. In particular, the CdS_xO sample presents an emerging asymmetric peak near 169 eV, referring to the SO₃^{2–}/SO₄^{2–} molecules,^{31,32} which provides evidence for the coupling SO_x^{2–} groups. These results unambiguously demonstrate evidence of surface conjugation of the sulfurous groups on CdS_xO NPs grown from the sulfur-rich solution.

Notably, Na₂S/Na₂SO₃ is usually employed as a sacrificing reagent to supply negatively charged S^{2–}/SO₃^{2–} ions dispersed in aqueous solution for the rapid capture of photogenerated holes, and thus make hot electrons more accessible into HER. However, the direct grafting of the S^{2–}/SO₃^{2–} groups on the catalysts has yet been underexplored for photocatalytic H₂ evolution. Therefore, it is worth examining whether the conjugated sulfurous groups can serve as hole-extraction chains, instead of expensive sacrificial agents, to reinforce the solar H₂ production over the present CdS_xO NP photocatalyst.

Photo-induced charge dynamics

The mean size of the CdS grains in the CdS_xO sample is estimated at *ca.* 6.5 nm using the Scherrer equation from the XRD data (Fig. S1, ESI[†]) and is consistent with the HR-TEM observation. In particular, this grain size is close to the depletion layer width (*W*, ~6.2 nm) estimated for n-type CdS (Note S1,

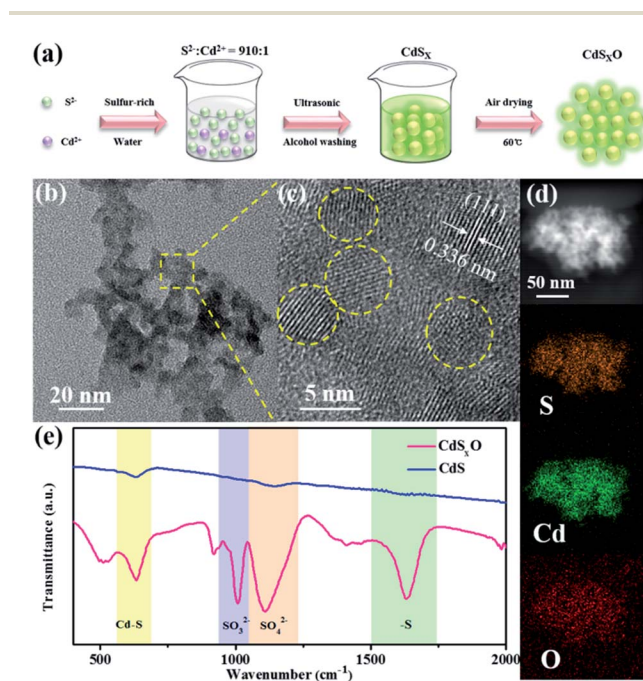


Fig. 1 Preparation and characterization. (a) Solvothermal synthetic route of CdS_xO NPs. (b) TEM image, (c) HR-TEM image, and (d) EDX elemental mappings of CdS_xO NPs. (e) FT-IR spectra of CdS_xO NPs and pure CdS crystals.

ESI[†]), and beyond the quantum-confined space defined by the Bohr exciton radius (R_B , ~ 3 nm).³³ Thus, the free diffusion in the absence of the interior electric force can be the main mechanism for the charge separation and outflow.³⁴ In fact, the high-proportion atoms near the surface in the small CdS grains play the main role in the photoelectronic excitation. Therefore, the separation and utilization of photogenerated electrons and holes can be governed by the kinetics of the surface charge transfer alone.³⁵ Here, the surface sulfurous groups on the CdS_xO NPs were designed as the capture buffer for hole extraction, resulting in the magnified charge separation and electron outflow. A series of photoelectron spectroscopies, including surface photovoltage (SPV), open-circuit potential (V_{oc}) decay and electron spin resonance (ESR), were performed to determine the properties of the photogenerated charge transfer. For comparison, the pure CdS sample composed of large particles ($D \sim 125$ nm, Fig. S9, ESI[†]) was obtained by the removal of the surface groups with annealing, in which the space charge region (SCR) exists near the surface of n-type CdS in depletion ($D > 2W$). In Fig. 2a, the CdS sample exhibits the weakly positive SPV signal with phase angles at the Ist quadrant; that is, the photogenerated holes are separated toward the surface.³⁶ This corresponds to the charge separation model by the in-built electric field in the surface SCR of the n-type depletion (Fig. 2g),³⁷ but the low SPV intensity reflects the very finite extent of the upward band bending that appears inadequate against the charge recombination kinetics. In contrast, the SPV signal of the CdS_xO sample is obviously negative with phase angles at the IInd quadrant; moreover, its absolute value is much larger than that of CdS. Thus, different from pure CdS, the photogenerated electrons in CdS_xO are efficiently concentrated on the surface upon the existence of sulfurous groups

that can quickly capture the out-diffusing holes from the CdS crystal cores (Fig. 2g). Accordingly, the ON/OFF switched SPV spectra (Fig. 2b) display the repeatable SPV responses that are vectorially opposite at two different samples and numerically different by a factor of 20. The SPV finding presents clear evidence for an important role of the surface conjugation with sulfurous groups in regulating the transfer of photogenerated charge, concomitant with the optimum charge separation and electron output.

The UV-vis absorption spectra in Fig. 2c show that both samples have a similar optical absorption dominated by the intrinsic band-gap charge transition in CdS, in which the slight blue shift of the absorption edge for CdS_xO is due to its composition of smaller CdS crystal grains (Fig. S10, ESI[†]). However, the two samples show the distinctly different intensities of photoluminescence (PL) associated with the band-gap charge recombination. By contrast, the obvious PL quenching effect for CdS_xO corresponds to a more favorable hole extraction upon surface sulfurous groups that efficiently restrains the recombination of the photogenerated electron-hole pairs. The transient V_{oc} decay was measured using an ON/OFF switched light illumination to examine the photo-induced charge dynamics.^{38,39} The temporal V_{oc} profile shows an evidently slower V_{oc} decay rate upon illumination termination for CdS_xO (Fig. S11, ESI[†]), which reflects the delaying kinetics of the charge recombination in CdS_xO relative to CdS. The calculated lifetime (τ) of the photogenerated electrons in CdS_xO is longer than that in CdS (Fig. 2d), and the prolonged electron survival indicates a more effective charge separation in CdS_xO as well. Spin-trapping experiments based on the ESR technique were employed to assess the relative amount of surface-reaching hot electrons.^{40,41} As shown in Fig. 2e, CdS_xO presents a set of strong ESR signals related to the spin adducts, confirming its high yield of separated electrons reaching the surface. In contrast, no ESR signal for the bare CdS sample identifies the difficulty of separated hot electrons reaching the surface in the absence of sulfurous groups. In addition, the Nyquist plots of electrochemical impedance spectroscopy (EIS, Fig. 2f) also show a smaller semicircle and better interfacial electron transfer in CdS_xO compared with bare CdS.

These abovementioned analyses on the photo-induced charge dynamics coherently demonstrate the kinetics acceleration of electron output from charge separation in CdS_xO NPs upon surface conjugation with sulfurous groups. The surface sulfurous groups consisting of negatively charged $-S/ SO_x^{2-}$ ions can reasonably work as hole traps to release electron overflows, which is favorable to instigate the photocatalytic reduction reaction (such as HER) and is similar to the function of hole sacrificial agents. However, it is conceivable that the limited sulfurous groups bonding on the surface cannot maintain the durable capture of photogenerated holes for photocatalytic HER application. The time-dependent photocurrent (Fig. S12a, ESI[†]) and bias voltage-dependent SPV (Fig. S13, ESI[†]) present the unstable photo-response signals associated with the disassembly of the sulfurous groups. To maintain the surface coordination with sulfurous groups, we introduced the UOR with low thermodynamic

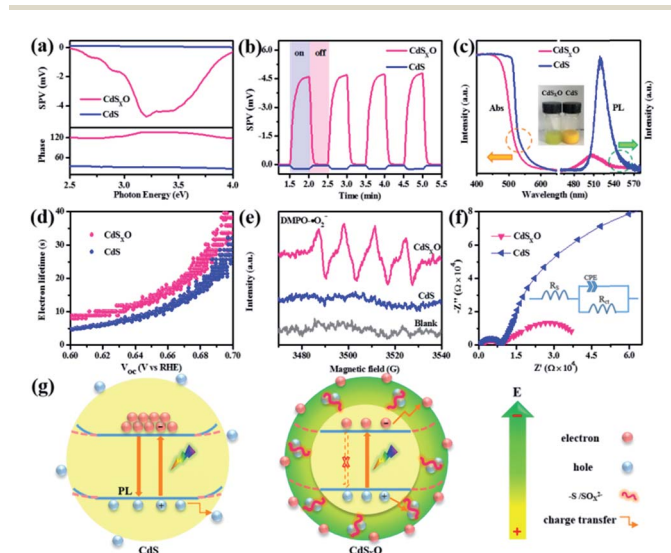


Fig. 2 Photo-induced charge dynamics. (a) SPV spectra with corresponding phase spectra, (b) ON/OFF switched SPV spectra, (c) absorption and PL spectra with corresponding samples' photographs (inset), (d) electron lifetime spectra, (e) electron-trapping ESR, (f) EIS spectra with an equivalent circuit model, and (g) schematic diagram for the photo-induced charge dynamic distribution in CdS and CdS_xO.

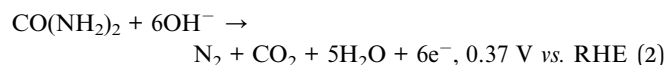
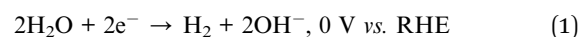
potential as the ultimate destination for the photogenerated holes, thereby making the surface sulfurous groups into durable mediators for hole transfer (Fig. S12b, ESI†). Of course, the downstream holes along the downhill thermodynamic potential will be incapable of triggering WOR, but the accelerated hole kinetics allow the optimum survival and output of hot electrons against charge recombination. Moreover, the consumption of holes into the UOR is also valuable for urea-rich wastewater purification.

Photocatalytic performance

Photocatalytic H₂ evolution experiments were performed with CdS and CdS_xO as catalysts in water without/with urea under simulated 1 sun irradiation (AM 1.5 G, 100 mW cm⁻²) without any additional sacrificial agents (Fig. 3a). The used dosages of the catalyst and urea were pre-optimized at 0.1 g L⁻¹ and 20 g L⁻¹, respectively, so as to maximize the photocatalytic performance (Fig. S14, ESI†). As expected, the pure CdS does not yield any detectable H₂ generation whether with or without urea due to the huge charge recombination. In the hole-capturing buffer of sulfurous groups, CdS_xO exhibits a definite proton reduction activity in pure water, which is especially rare in the absence of sacrificial agents, reflecting the well-steered charge transfer toward HER. When integrating with UOR, CdS_xO shows a significantly enhanced HER activity with a H₂-evolution rate of up to 1.49 mmol h⁻¹ g⁻¹ (Fig. 3b) and an AQY as high as 2.4% at 420 nm (Note S2 and Fig. S15, ESI†), which are competitive with

those reported in recent literature (Table S2, ESI†).^{42–46} Although the UOR involvement can promote the activity of CdS_xO, this effect does not work well on pure CdS, which indicates that the role of the surface sulfurous groups in manipulating the charge dynamics is of crucial importance for charge distribution into catalytic redox reactions. For example, when using Na₂S/Na₂SO₃ or lactic acid (LA) as the hole sacrificial agents, pure CdS only displays a little bit of activity, whereas CdS_xO renders an outstanding activity growth (Fig. S16, ESI†). This further proves the desirable regulation of the surface sulfurous groups on charge transfer and separation, which cannot be imitated by dissociative sulfurous ions in a Na₂S/Na₂SO₃ solution.

Moreover, in addition to the enhanced H₂ generation, a simultaneous urea degradation is demonstrated with nitrogen (N₂) generation detected by gas chromatography. As expected, CdS presents a negligible N₂ evolution activity, while CdS_xO enables a N₂-evolution rate of up to 0.5 mmol h⁻¹ g⁻¹, corresponding to urea degradation. The relevant reactions during H₂ generation with simultaneous urea degradation are as follows:



Notably, the measured evolution rates of H₂ and N₂ at a stoichiometric ratio of 3 : 1 match well with an integrated redox reaction with HER and UOR by electron exchange. The mild UOR alternative to the harsh WOR can shift the thermodynamic potential from 1.23 V to a mere 0.37 V, lowering the photovoltaic standard of solar-to-H₂ conversion.

The photocatalytic stability of CdS_xO for H₂ evolution with simultaneous urea degradation was examined by cycling experiments. Continuous H₂ and N₂ production was observed with no significant decay in the sequential runs (Fig. 3d and e). Moreover, the CdS_xO catalyst still maintained a similarly high catalytic activity after storage for one week. In addition, the TEM image, XRD pattern, Raman and EDX spectra of the CdS_xO catalyst after stability testing are recorded in Fig. S17 (ESI†). Altogether, the results show no noticeable change compared with those before use. These results support the promising application of CdS_xO NPs as an efficient and robust photocatalyst for solar H₂ production from urea-rich wastewater. In particular, the activity decay is observed for cycling H₂ evolution over CdS_xO in pure water without urea (Fig. S18, ESI†), implying the disassembly of sulfurous groups under hole accumulation. Therefore, the mild UOR can change the role of the surface sulfurous groups from a hole collector to mediator with transfer acceleration; on the other hand, the surface sulfurous groups can operate hole capture and transfer toward UOR against strong charge recombination kinetics. The sulfur atoms with multiple-charged permissible states in the sulfurous groups enable the charge transfer mediation, and the formed inter-band energy levels (by surface states) built fast channels of hole transfer toward UOR. The proposed charge transfer mechanism is schematically depicted in the energy band structure established by estimating the bandgap and flatband potentials

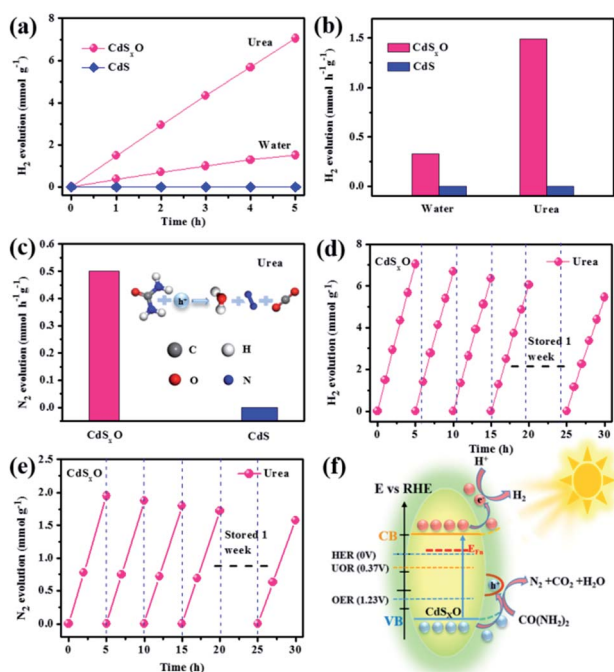


Fig. 3 Photocatalytic performance. (a) Time courses of H₂ evolution, (b) H₂-evolution rates, (c) N₂-evolution rates with urea degradation, (d) H₂-evolution, and (e) N₂-evolution stabilities in cycling runs for CdS_xO and CdS as catalysts in water without/with urea under simulated 1 sun irradiation. (f) Schematic diagram for photo-induced charge dynamics with HER and UOR on CdS_xO.

(Fig. S19, ESI†). As shown in Fig. 3f, both types of photo-generated charge carriers are separately steered toward the specified redox reactions by hole dynamics modulation, enabling an improved solar H₂ production with simultaneous urea photolysis.

Conclusions

In summary, we report a strategy of modulating hole dynamics to improve solar H₂ production by engineering surface conjugation and alternative oxidation reaction. Thereby, CdS_xO NPs conjugated with sulfurous groups have been developed as an efficient and robust photocatalyst for solar H₂ production from urea-rich wastewater with synchronous urea degradation. The surface sulfurous groups are demonstrated to function as a hole-capturing buffer that transports holes downstream into the thermodynamically mild UOR, enabling the hole-transfer acceleration for the optimum separation and utilization of the photogenerated charge into specified redox reactions. The photocatalytic H₂ generation over the CdS_xO NPs reaches an impressive rate of 1.49 mmol h⁻¹ g⁻¹ under 1 sun irradiation with an AQY up to 2.4% at 420 nm. This study not only provides an interesting waste-to-energy solution, but also gains deep insight into the charge dynamics for photocatalytic H₂ generation.

Methods

Sample synthesis

CdS_xO NPs were prepared through a facile co-solvent method with a tunable ratio of Cd(OAc)₂ and Na₂S as the Cd and S sources, followed by extraction washing and air drying. In a typical procedure, 4 g of Na₂S first was added into 40 mL of distilled water. The dispersion was sonicated by a sonicator (Misonix XL-2000) for 10 min with an output power of 150 W. Second, a 2 mL aqueous solution of 7.5 g L⁻¹ Cd(OAc)₂·2H₂O was added into a sulfur-rich Na₂S solution, and then sonicated for 10 min. The products were collected using centrifugation at 12 000 rpm for 3 min and washed several times with deionized (DI) water and absolute ethanol to remove the residues of other ions. The final products were dried at 60 °C overnight. For comparison, the pure CdS crystals were synthesized by calcining the CdS_xO sample at 550 °C for 4 h in a tubular furnace under argon blanketing to remove the surface groups. In addition, the CdS_xO samples with different contents of surface sulfurous groups were synthesized by the same procedure with the exception of adding different dosages of Na₂S (from 4.7 mg to 5 g). Based on the photocatalytic activity maximum, the ratio of Cd and S ions was optimized to 1 : 910, and the resultant CdS_xO NPs were bright yellow in color (Fig. S20, ESI†).

Characterization

TEM and HR-TEM characterizations were performed using a Tecnai F30 electron microscope equipped with EDX spectroscopy at an acceleration voltage of 300 kV. XRD measurements were conducted on the Shimadzu XRD-7000 diffractometer with Cu Kα radiation ($\lambda = 0.15406$ nm) to study

the crystal structure and the phase composition. FT-IR spectroscopy was conducted using a Varian Cary 670 spectrometer. XPS measurements were carried out on an ESCALAB 250Xi spectrometer with a monochromatic Al Kα X-ray source operating at 150 W, and the binding energies were calibrated according to the C 1s peak at 284.78 eV. Raman spectra were measured using a research laser Raman microscope (Renishaw inVia) with an incident 532 nm laser of 300 mW, and the steady-state PL spectra were recorded at room temperature using a research laser Raman microscope (Renishaw inVia) with an incident 325 nm laser of 300 mW. SPV measurements were performed with a monochromatic light source (CHF-XM-500 W, Global Xenon Lamp Power) through grating monochromator (Omni-λ3007-MC300) and lock-in amplifier (SR830-DSP) with light chopper (SR540) at a chopping frequency of 23 Hz. UV-vis absorption spectra were recorded with a Cary 5000 spectrophotometer (Varian). DMPO spin-trapping ESR spectra were measured on an A300-10/12 instrument for different catalysts (5 mg) dispersed in 1.5 mL CH₃OH with 50 μL of DMPO to examine the superoxide radical adducts (DMPO-O₂⁻).

PEC measurement

PEC measurements were performed on an electrochemical workstation (CHI660C Instruments, Shanghai, China) in a standard three-electrode system with the catalyst-coated FTO (2 × 1.5 cm²) as the working electrode, an Ag/AgCl and a graphite rod were used as the reference and counter electrodes, respectively. The working electrodes were prepared by dropping the suspensions (30 μL) made of various catalysts (1 mg catalysts added into 50 μL Nafion and 450 μL ethanol mixed solution, respectively) onto the FTO plates. The electrodes were dried with N₂ atmosphere at room temperature. The aqueous solutions without/with 0.33 M urea were used as the electrolytes. The potentials were calibrated with respect to the reversible hydrogen electrode (RHE) according to $E(\text{RHE}) = E(\text{Ag}/\text{AgCl}) + 0.599$ V at pH = 6.8. The “1 Sun” illumination was simulated by a 300 W Xe short arc lamp solar simulator (PerfectLight, Beijing, PLS-SXE 300C) with an AM 1.5 G filter. The light intensity was calibrated to 100 mW cm⁻² by an irradiometer (Beijing, FZ-A). The photocurrent responses of the electrodes were measured under chopped irradiation at 0 V vs. RHE.

Photocatalytic measurement

Photocatalytic H₂ evolution experiments were performed in a closed gas circulation and evacuation system fitted with a top window of optical flat quartz glass (Labsolar-IV (AG), PerfectLight, Beijing). The suspension was then stirred in a sealed glass vessel and purged with Ar for 30 min prior to photocatalytic experiments to remove dissolved oxygen. The vials were placed in a thermoregulated rack at 26 °C with magnetic stirring, and then irradiated by the simulated solar light from the Xe lamp with an AM 1.5 G filter. The focused light power intensity (I_i) on the reactor was uniformly calibrated to 100 mW cm⁻². The amounts of evolved H₂ and N₂ gases were measured by an online gas chromatography (9790 II, Fuli, Zhejiang) with a thermal conductivity detector (TCD) and Ar as carrier gas.

Different samples (CdS_xO and CdS) with the same mass were respectively used as catalysts dissolved into 100 mL aqueous solutions without/with urea. The dosages of catalyst and urea were pre-optimized at 0.1 g L⁻¹ and 20 g L⁻¹ based on the photocatalytic performance maximum. The photocatalytic stability was evaluated by extracting, washing, and reusing the catalyst with centrifugation in cycling experiments. The AQY was defined by the following eqn (3), and was measured using a 300 W Xe lamp with 400 and 420 nm (±5 nm) band-pass filter and an irradiatometer (FZ-A, Perfectlight, Beijing). The detailed calculations are shown in the Note S2 and Fig. S15 (ESI†).

$$\begin{aligned} \text{AQY}[\%] &= \frac{\text{number of reacted electrons}}{\text{number of incident photons}} \times 100\% \\ &= \frac{\text{number of evolved H}_2 \text{ molecules} \times 2}{\text{number of incident photons}} \times 100\% \quad (3) \end{aligned}$$

Conflicts of interest

There are no conflicts to declare.

Acknowledgements

This study was financially supported by the National Natural Science Foundation of China (11974303, 11574263 and 11674276), the National Basic Research Program of China (2014CB931702), the Qinglan Project of Jiangsu Province, and the Personnel Plan of Yangzhou University and Hangzhou Dianzi University.

References

- L. F. Pan, J. H. Kim, M. T. Mayer, M. K. Son, A. Ummadisingu, J. S. Lee, A. Hagfeldt, J. Luo and M. Grätzel, *Nat. Catal.*, 2018, **1**, 412.
- C. Niether, S. Faure, A. Bordet, J. Deseure, M. Chatenet, J. Carrey, B. Chaudret and A. Rouet, *Nat. Energy*, 2018, **3**, 476.
- T. Hisatomi, J. Kubota and K. Domen, *Chem. Soc. Rev.*, 2014, **43**, 7520.
- J. Gong, C. Li and M. R. Wasielewski, *Chem. Soc. Rev.*, 2019, **48**, 1862.
- X. Yang, L. Tian, X. Zhao, H. Tang, Q. Liu and G. Li, *Appl. Catal., B*, 2019, **244**, 240.
- X. Wang, L. Chen, S. Y. Chong, M. A. Little, Y. Wu, W. H. Zhu, R. Clowes, Y. Yan, M. A. Zwiijnenburg, R. S. Sprick and A. I. Cooper, *Nat. Chem.*, 2018, **10**, 1180.
- R. Chen, S. Pang, H. An, J. Zhu, S. Ye, Y. Gao, F. Fan and C. Li, *Nat. Energy*, 2018, **3**, 655.
- Z. Lan, W. Ren, X. Chen, Y. Zhang and X. C. Wang, *Appl. Catal., B*, 2019, **245**, 596.
- J. Guan, Z. Duan, F. Zhang, S. D. Kelly, R. Si, M. Dupuis, Q. Huang, J. Q. Chen, C. Tang and C. Li, *Nat. Catal.*, 2018, **1**, 870.
- P. Li, X. Chen, H. He, X. Zhou, Y. Zhou and Z. Zou, *Adv. Mater.*, 2018, **30**, 1703119.
- Y. Kuang, T. Yamada and K. Domen, *Joule*, 2017, **1**, 290.
- S. Bai, J. Jiang, Q. Zhang and Y. Xiong, *Chem. Soc. Rev.*, 2015, **44**, 2893.
- B. You, X. Liu, N. Jiang and Y. Sun, *J. Am. Chem. Soc.*, 2016, **138**, 13639.
- Z. Yu, C. Lang, M. Gao, Y. Chen, Q. Fu, Y. Duan and S. H. Yu, *Energy Environ. Sci.*, 2018, **11**, 1890.
- B. You, N. Jiang, X. Liu and Y. Sun, *Angew. Chem., Int. Ed.*, 2016, **55**, 9913.
- J. Han, X. Zheng, L. Zhang, H. Fu and J. Chen, *Environ. Sci.: Nano*, 2017, **4**, 834.
- X. Zhu, X. Dou, J. Dai, X. An, Y. Guo, L. Zhang, S. Tao, J. Zhao, W. Chu, X. C. Zeng, C. Wu and Y. Xie, *Angew. Chem., Int. Ed.*, 2016, **55**, 12465.
- T. Take, K. Tsurutani and M. Umeda, *J. Power Sources*, 2007, **164**, 9.
- C. Tang, R. Zhang, W. Lu, Z. Wang, D. Liu, S. Hao, G. Du, A. M. Asiri and X. Sun, *Angew. Chem., Int. Ed.*, 2017, **56**, 842.
- M. Song, Z. Zhang, Q. Li, W. Jin, Z. Wu, G. Fu and X. Liu, *J. Mater. Chem. A*, 2019, **7**, 3697.
- C. Li, Y. Liu, Z. Zhuo, H. Ju, D. Li, Y. Guo, X. Wu, H. Li and T. Zhai, *Adv. Energy Mater.*, 2018, **8**, 27.
- Y. Liang, Q. Liu, A. M. Asiri and X. Sun, *Electrochim. Acta*, 2015, **153**, 456.
- K. H. Cho and Y. M. Sung, *Nano Energy*, 2017, **36**, 176.
- R. Shi, H. F. Ye, F. Liang, Z. Wang, K. Li, Y. Weng, Z. Lin, W. Fu, C. Che and Y. Chen, *Adv. Mater.*, 2018, **30**, 1705941.
- L. Cheng, Q. Xiang, Y. Liao and H. Zhang, *Energy Environ. Sci.*, 2018, **11**, 1362.
- H. Yu, W. Zhong, X. Huang, P. Wang and J. G. Yu, *ACS Sustainable Chem. Eng.*, 2018, **6**, 5513.
- Y. Zhang, L. Han, C. Wang, W. Wang, T. Ling, J. Yang, C. Dong, F. Lin and X. W. Du, *ACS Catal.*, 2017, **7**, 1470.
- S. K. Verma, M. K. Deb and J. Agric, *Food Chem.*, 2007, **55**, 8319.
- N. R. Yogamalar, K. Sadhanandam, A. C. Bose and R. Jayavel, *RSC Adv.*, 2015, **5**, 16856.
- F. Vaquero, R. M. Navarro and J. L. G. Fierro, *Appl. Catal., B*, 2017, **203**, 753.
- X. Zheng, J. Xu, K. Yan, H. Wang, Z. Wang and S. Yang, *Chem. Mater.*, 2014, **26**, 2344.
- J. D. Benck, Z. B. Chen, L. Y. Kuritzky and A. J. Forman, *ACS Catal.*, 2012, **2**, 1916.
- J. M. Catherine, *J. Cluster Sci.*, 1996, **7**, 341.
- F. E. Osterloh, *Chem. Soc. Rev.*, 2013, **42**, 2294.
- G. Hodes, I. D. J. Howell and L. M. Peter, *J. Electrochem. Soc.*, 1992, **139**, 3136.
- S. Li, D. Meng, L. Hou, D. J. Wang and T. F. Xie, *Appl. Surf. Sci.*, 2016, **371**, 164.
- J. Zhu, S. Pang, T. Dittrich, Y. Gao, W. Nie, J. Cui, R. Chen, H. An, F. Fan and C. Li, *Nano Lett.*, 2017, **17**, 6735.
- J. H. Bang and P. V. Kamat, *Adv. Funct. Mater.*, 2010, **20**, 1970.
- J. Li, Q. Pei, R. Wang, Y. Zhou, Z. Zhang, Q. Cao, D. H. Wang, W. B. Mi and Y. W. Du, *ACS Nano*, 2018, **12**, 3351.

- 40 C. Zhao, Z. Chen, J. Xu, Q. Liu, H. Xu, H. Tang, G. Lie, Y. Jiang, F. Qu, Z. Lin and X. Yang, *Appl. Catal., B*, 2019, **256**, 117867.
- 41 Q. Liu, J. Shen, X. Yu, X. Yang, W. Liu, J. Yang, H. Tang, H. Xu, H. Li, Y. Li and J. Xu, *Appl. Catal., B*, 2019, **248**, 84.
- 42 J. Xu, X. Li, Z. Ju, Y. Sun, X. Jiao, J. Wu, C. Wang, W. Yan, H. Ju, J. Zhu and Y. Xie, *Angew. Chem., Int. Ed.*, 2019, **131**, 3064.
- 43 M. Zhu, Z. Sun, M. Fujitsuka and T. Majima, *Angew. Chem., Int. Ed.*, 2018, **57**, 2160.
- 44 G. Zhou, Y. Shan, Y. Hu, X. Xu, L. Long, J. Zhang, J. Dai, J. Guo, J. Shen, S. Li, L. Liu and X. Wu, *Nat. Commun.*, 2018, **9**, 3366.
- 45 Z. M. Pan, G. G. Zhang and X. C. Wang, *Angew. Chem., Int. Ed.*, 2019, **131**, 7176.
- 46 Y. Lu, W. Yin, K. Peng, K. Wang, Q. Hu, A. Selloni, F. Chen, L. Liu and M. L. Sui, *Nat. Commun.*, 2018, **9**, 2752.